Physicochemical Characterization of Mixed RuO_2-SnO_2 Solid Solutions

J. Gaudet,[†] A. C. Tavares,[‡,§] S. Trasatti,[‡] and D. Guay*[,†]

INRS-Énergie, Matériaux et Télécommunications, 1650 Blvd. Lionel Boulet, C. P. 1020,Varennes, Quebec, Canada J3X 1S2, and Department of Physical Chemistry and Electrochemistry, University of Milan, Via Venezian 21, 20133 Milan, Italy

Received October 26, 2004. Revised Manuscript Received January 14, 2005

Mixed SnO_2-RuO_2 oxides were prepared by high-energy mechanical alloying of various proportions of pure SnO_2 and RuO_2 powders. The physicochemical characterization of the resulting materials was conducted by X-ray diffraction (XRD), scanning electron microscopy (SEM), X-ray photoelectron spectroscopy (XPS), and electrochemical surface analysis. It is shown through XRD analysis that a single-phase (tetragonal) $(Sn-Ru)O_2$ solid solution is formed over the whole composition range, in which the Sn^{4+} and Ru^{4+} ions share the same cationic sub-lattice of the rutile-like structure. The surface of the compounds was analyzed by XPS and shows a deficit of Ru atoms, with $[Ru]_{surface} = 36$ at. % for an equimolar SnO_2-RuO_2 concentration in the bulk of the sample. In the case of pure nanocrystalline RuO_2, the total surface charge, q_T*, the most easily accessible surface charge, q_O*, and the less easily accessible surface charge, q_I*, are 35.3, 29.0, and 6.3 mC cm^{-2} mg^{-1}, respectively. These surface charges vary linearly with the Ru content at the surface of the electrode, indicating that the surface electrochemical properties of the compounds are dominated by the redox properties of the Ru^{4+} cation. The ratio q_O*/q_T* is close to 0.8 and independent of the surface composition, suggesting that all compounds have a similar morphology.

Introduction

Dimensionally stable anodes (DSAs) are used in a variety of electrode processes including chlor-alkali and water electrolysis, metal electrowinning, organic syntheses, oxidation of organics, etc.[1−4] The terminology "dimensionally stable anode" emphasizes the stability of these electrodes toward chemical and electrochemical deterioration. DSAs consist of an active transition metal oxide (RuO_2, IrO_2, Co_3O_4, perovskites, etc.) stabilized by a valve metal oxide (typically TiO_2, ZrO_2, SnO_2, Ta_2O_5, etc.). Although DSAs can be prepared by a variety of deposition processes, thermal decomposition is still the method of choice because it lends itself especially well to the deposition of the oxide as a thin layer at the surface of a substrate.

The purpose of using mixed oxides is to modulate the electrochemical properties of the active layer by modifying its composition. Various outcomes can be reached, depending on the degree of mixing of the constituent oxides. The properties of the pure oxides may add up proportionally to their content if a phase mixture is obtained, while a true synergistic effect can be expected if intimate mixing (solid solution) is achieved.

Electrodes made from mixtures of RuO_2 and SnO_2 were first studied at the end of the 1970s and the beginning of the 1980s by Chertykovtseva et al.,[5] Iwakura et al.,[6−8] and Bondar et al.[9] Much of the interest generated by these first studies stems from the fact that mixed SnO_2-RuO_2 oxide coatings show improved electrocatalytic activity for chlorine evolution over doped SnO_2 electrodes.[5] In the case of chlorine evolution, the molar activity shows a maximum as a function of RuO_2 loading, indicative of the presence of a synergistic effect.[7] In the case of oxygen evolution, the molar activity is independent of the RuO_2 loadings, indicating that SnO_2 acts as an inert support.[7] The effect of the active layer composition on the service life of (SnO_2 + RuO_2)-coated Ti electrodes was studied in acidic solution. It was shown that the presence of SnO_2 in the active coating considerably increases cthe service life of the electrode, with a maximum at around 30 mol % RuO_2.[10] Since then, the idea of adding SnO_2 to modify and improve the coating performances has been played several times in the literature (IrO_2 + SnO_2,[11,12] IrO_2 + RuO_2 + SnO_2,[13] RuO_2 + TiO_2 + SnO_2,[14−17]], IrO_2 + TiO_2 + SnO_2,[18]and RuO_2 + SnO_2).[19−22]

* To whom correspondence should be addressed.
[†] NRS-Énergie.
[‡] University of Milan.
[§] Present address : Pirelli Labs (Materials Innovation), Viale Sarca 222, 20126 Milan, Italy.

(1) Trasatti, S., Ed. *Electrodes of Conductive Metallic Oxides*, Part A and Part B: Elsevier: Amsterdam, 1980−1981.
(2) Trasatti, S., Lipkowski, J., Ross, P. N., Eds. *Electrochemistry of Novel Materials*; VCH: Weinheim, 1994; p 207.
(3) Trasatti, S. *Electrochim. Acta* **1991**, *36*, 225.
(4) Ch. Comninellis De Battisti, A. *J. Chem. Phys.* **1996**, *93*, 673.
(5) Chertykovtseva, T. A.; Skuridina, Z. D.; Shub, D. M.; Veselovskii, V. I. *Elecktrokchimiya* **1978**, *14*, 1412.
(6) Iwakura, C.; Inai, M.; Tamura, H. *Chem. Lett.* **1979**, 225.
(7) Iwakura, C.; Taniguchi, Y.; Tamura, H. *Chem. Lett.* **1981**, 689.
(8) Iwakura, C.; Inai, M.; Uemura, T.; Tamura, H. *Electrochim. Acta* **1981**, *26*, 579.
(9) Bondar, R. U.; Kalinovskii, E. A.; Kunpan, I. V.; Sorokendya, V. S. *Electrokchimiya* **1983**, *19*, 1104.
(10) Iwakura, C.; Sakamoto, K. *J. Electrochem. Soc.* **1985**, *132*, 2420.
(11) Balko, E. N.; Nguyen, P. H. *J. Appl. Electrochem.* **1991**, *21*, 678.
(12) De Pauli, C. P.; Trasatti, S. *J. Electroanal. Chem.* **1995**, *396*, 161.
(13) Hutchings, R.; Müller, K.; Kötz, R.; Stucki, S. *J. Mater. Sci.* **1984**, *19*, 3987.

10.1021/cm048129l CCC: $30.25
Published on Web 02/19/2005

Tin and ruthenium dioxide crystallize in the same tetragonal (rutile-like) structure. The lattice parameters of SnO_2 and RuO_2 are quite close to each other (SnO_2, $a = 4.7382$ and $c = 3.1871$ Å; RuO_2, $a = 4.4994$ and $c = 3.1071$ Å). From a theoretical viewpoint, the ionic radius of Sn^{4+} is 0.083 nm, considerably larger than that of Ru^{4+} (0.076 nm). However, it still lies just within the Hume−Rothery limit for successful substitution. Accordingly, it may be possible to form a solid solution of SnO_2 and RuO_2, whereby Ru^{4+} and Sn^{4+} share the same site on the cationic sub-lattice of a tetragonal (rutile-like) phase.

Indeed, there is some evidence in the literature that a RuO_2−SnO_2 solid solution can be prepared,[10,19,22] although the exact phase composition varies greatly with the details of the preparation procedure. For example, it was shown that coatings of mixed SnO_2−RuO_2 prepared by thermal decomposition over a limited period of time contain two oxide phases, with one richer in RuO_2 than the other one.[22] However, coatings of similar composition prepared according to a slightly different procedure do not exhibit this dual-phase composition. Instead, the shape of the (110) diffraction peak suggests that a single-phased material is formed.[10] However, the change in the (110) peak position with the RuO_2 content does not correspond to what is expected if a true RuO_2−SnO_2 solid solution is formed over the whole composition range.[10] Ultrafine particles of RuO_2−SnO_2 binary oxides were also prepared by a sol−gel process consisting of hydrolysis and condensation of metal alkoxide alcoholic solutions.[19] However, this preparation method failed to yield a single-phase material and the presence of metallic Ru was pointed out in some samples.

Part of the difficulty faced in preparing a single-phase material consisting of a true RuO_2−SnO_2 solid solution over a wide composition range may be related to the preparation procedure itself. In the thermal decomposition method, it is well-known that bulk phase compositions, as well as electrode surface compositions, are influenced by the oxidation and the precipitation kinetics of the two (or more) dissimilar metallic ions. Very small modifications of the experimental protocol (solvent used to dissolve salt precursors, heating rate, thickness of each layer, etc.) have a strong influence on the physicochemical characteristics of the oxide coatings and thus on their electrochemical response.[3] In these conditions, it is difficult to ascertain the intrinsic electrochemical properties of mixed SnO_2−RuO_2 oxide without going into a lengthy characterization of the electrodes as the exact bulk phase and surface compositions may vary greatly according to very fine details of the preparation procedure. Clearly, an alternative and more reliable way to prepare single-phased SnO_2−RuO_2 binary oxides over as wide a composition range as possible must be explored.

High-energy ball milling (HEBM) is known as an effective means of preparing nonequilibrium and metastable phases, amorphous alloys, supersatured solid solutions, and nanocomposites. Comprehensive review articles on HEBM can be found in the literature and, for example, the interested reader should consult references 23−26. In summary, high-energy mechanical alloying by ball-milling consists of inducing a solid-state reaction between the components of a powder mixture by repeated mechanical deformations. During milling, numerous structural defects are created which increase the interatomic diffusion, thereby allowing a solid-state reaction to proceed. Also, strain is introduced in the lattice during milling, which results in crystal breaking into smaller pieces down to the nanometer range.

In the present study, SnO_2−RuO_2 binary oxides were prepared by high-energy ball milling over the whole composition range. The oxides were characterized by powder X-ray diffraction, scanning electron microscopy, and X-ray photoelectron spectroscopy. It will be shown that prolonged milling of SnO_2 and RuO_2 yields to the formation of a single-phased material which is a true $(Sn-Ru)O_2$ solid solution, whereby the Sn^{4+} and Ru^{4+} ions occupy the same site on the cationic sub-lattice. Some basic electrochemical properties of these oxides will also be reported.

Experimental Section

Materials. Mixed SnO_2−RuO_2 oxides were prepared by continuous milling of SnO_2 and RuO_2 powders. The milling operation was performed with a SPEX-8000 shaker mill under an air atmosphere. Commercial $RuO_2 \cdot xH_2O$ (from Aldrich) was first heated at 700 °C during 16 h to remove the structural water molecules present in the as-received material. Then, SnO_2 (from Aldrich) and crystalline RuO_2 were milled together with two WC balls (diameters of 15.8 and 12.4 mm) in a WC crucible (volume of 53 cm^3). Mixed SnO_2−RuO_2 oxides were prepared by varying the composition of the initial powder mixture from $[RuO_2] = 0$ to 100 wt. % by steps of 20 wt. %.

Electrodes. The electrodes were fabricated by first preparing slurries made from the oxide material, water, and 10 wt. % Teflon (Aldrich, dispersion of 60 wt. % of polytetrafluorethylene in water). This slurry was then painted on both sides of pretreated Ti platelets. Each slurry layer was dried under a nitrogen flow before the application of the next layer. The operation was repeated several times. The total mass of the deposit was between 4 and 8 mg. The electrode surface covered by the oxide was 2 cm^2. The pretreatment of the Ti platelets consisted of first polishing the Ti substrate with an emery paper and then etching the platelet during 1 h in a 0.8 mol dm^{-3} oxalic acid solution.

Physical Characterization. The crystalline structure of the powders was determined by powder X-ray diffraction (XRD) in the Bragg−Brentano ($\theta/2\theta$) configuration. The powder X-ray

(14) Shieh, D. T.; Hwang, B. J. *Electrochim. Acta* **1993**, *38*, 2239.
(15) Bandi, A.; Vartires, I.; Mihelis, A.; Hainăşrosie, C. *J. Electroanal. Chem.* **1983**, *157*, 241.
(16) Boodts, J. F. C.; Trasatti, S. *J. Electrochem. Soc.* **1990**, *137*, 3784.
(17) Onuchukwu, A. I.; Trasatti, S. *J. Appl. Electrochem.* **1991**, *21*, 858.
(18) Lassali, T. A. F.; Bulhões, L. O. S.; Abeid, L. M. C.; Boodts, J. F. C. *J. Electrochem. Soc.* **1997**, *144*, 3348.
(19) Badawy, W.; Doblhofer, K.; Eiselt, I.; Gerischer, H.; Krause, S.; Melsheimer, J. *Electrochim. Acta* **1984**, *29*, 1617.
(20) Ito, M.; Murakami, Y.; Kaji, H.; Ohkawauchi, H.; Yahikozawa, K.; Takasu, Y. *J. Electrochem. Soc.* **1994**, *141*, 1243.
(21) Ito, M.; Murakami, Y.; Kaji, H.; Yahikozawa, K.; Takasu, Y. *J. Electrochem. Soc.* **1996**, *143*, 32.
(22) Nanni, L.; Polizzi, S.; Benedetti, A.; De Battisti, A. *J. Electrochem. Soc.* **1999**, *146*, 220.
(23) Koch, C. C. *Annu. Rev. Mater. Sci.* **1989**, *19*, 121.
(24) Suryanarayana, C., Ed. *Nonequilibrium Processing of Materials*; Pergamon: New York, 1999.
(25) Koch, C. C.; Whittenberger, J. D. *Intermetallics* **1996**, *4*, 339.
(26) Suryanarayana, C. *Bibliography on Mechanical Alloying and Milling*; Cambridge Interscience: Cambridge, U.K., 1995.

diffraction histograms were measured on a Bruker D8 instrument using Cu Kα radiation. Scanning electron microscopy (SEM) micrographs were obtained using a Hitachi S-4700 instrument operated at 15 kV. Chemical analysis was performed by energy-dispersive X-ray spectroscopy (EDX). Surface analysis was obtained by X-ray photoelectron spectroscopy (XPS) on a VG Escalab 220i-XL equipped with Al Kα monochromatic source and a hemispherical analyzer with a multichannel detector. Repeated measurements over the same area did not show any evidence of damage caused by effects induced by X-ray irradiation on the sample.

Electrochemical Measurements. All experiments were carried out in 0.5 mol dm^{-3} H_2SO_4 solution prepared using distilled water of Milli-Q quality. A three-compartment electrochemical cell was used to perform the measurements. This cell has been described elsewhere.[27] Platinum was used as counter electrode. Electrode potentials were measured and recorded against a saturated calomel electrode. All experiments were performed with AMEL instrumentation (model 2053 potentiostat, model 568 function generator). The potentiostat support system was Voltassist advanced 2.0. For the determination of the electrochemical surface properties, voltammetric curves were recorded between 0.05 and 1.05 V (ECS) at the following scan rates: 1, 2, 3, 5, 7, 10, 15, 20, 30, 40, 50, 60, 80, 100, 150, 200, 250, and 300 mV s^{-1}. For the determination of the electrocatalytic activity toward oxygen evolution, a Tafel study was performed, with quasi-stationary polarization curves recorded between 1.1 and 1.4 V at 0.1667 mV s^{-1}. Curves were recorded until forward (from lower to higher electrode potential) and backward (from higher to lower electrode potential) scans were superimposed on each other.

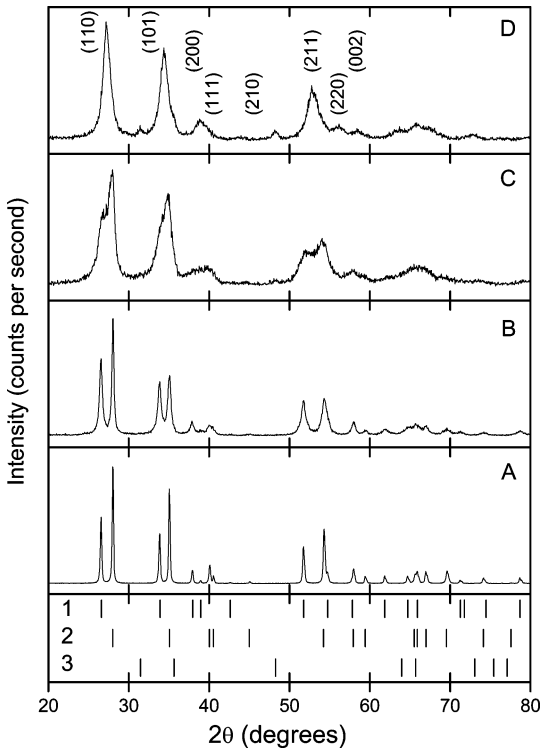

Figure 1. XRD patterns of mixed SnO_2-RuO_2 (50:50 wt. %) as a function of milling times: (A) 0 h, (B) 1 h, (C) 11 h, and (D) 40 h. The positions of the diffraction peaks of SnO_2 (1), RuO_2 (2), and WC (3) are indicated at the bottom.

Results and Discussion

Structural Characterization. The powder XRD patterns of mixed SnO_2-RuO_2 (50−50 wt. %) at various milling times are shown in Figure 1. SnO_2 and RuO_2 crystallize with the same tetragonal structure. The lattice parameters of SnO_2 are $a = 4.7382$ and $c = 3.1871$ Å (JCPDS 41-1445), while those of RuO_2 are $a = 4.4994$ and $c = 3.1071$ Å (JCPDS 40-1290). There is thus a close similarity between the histograms of these two compounds (see curve A).

After 1 h of milling (curve B), the individual diffraction peaks of SnO_2 and RuO_2 are still clearly discernible, indicating that both phases coexist. However, the diffraction peaks are larger than those in the starting material, indicating that refinement of the crystallite size has already started. Upon further milling (11 h, curve C), the width of the diffraction peaks increases further and the corresponding (*hkl*) diffraction peaks of SnO_2 and RuO_2 merge into one another. The individual diffraction peaks of SnO_2 and RuO_2 are no longer observed after 40 h of milling (curve D). Instead, a unique set of peaks is observed, the sequencing of which is reminiscent of that of a tetragonal structure similar to that of the starting oxides. After 40 h of milling, the positions of the various (*hkl*) peaks fall between those of the corresponding peaks of SnO_2 and RuO_2. This suggests that the lattice parameters *a* and *c* of the tetragonal phase of the end material are intermediate between those of SnO_2 and RuO_2. Curve D of Figure 1 also displays small diffraction peaks belonging to WC coming from the attrition of the milling tools. Identical results were obtained when the milling operation was performed with a steel crucible and steel balls, suggesting that WC is not involved in the formation of the new tetragonal structure.

The evolution with time of the powder XRD patterns of the 50−50 wt % mixture of SnO_2 and RuO_2 is shown in Figure 2 for a restricted 2θ region centered on the (110) diffraction peak. The fitting of that part of the histograms was performed assuming the milled powder is composed of three different components (SnO_2, RuO_2, and a newly formed oxide phase). A pseudo-Voigt function was used to simulate the peak shape of each component. Each function has four independent parameters, namely xc (position of the peak maximum), *A* (area), *w* (width at half-maximum), and μ (ratio between the Gaussian and Lorentzian part of the function). The background was estimated by using a linear function. As can be seen in Figure 2, the agreement between the experimental data and the fitting curve is excellent in all cases.

The relative concentration of the three components, as given by the relative percent area under the three peaks, is shown with respect to the milling time in the upper panel of Figure 3. There is a steady decrease of the area under the (110) peak of SnO_2 and RuO_2, while the area under the (110) peak of the new phase increases. After 40 h of milling, the diffraction peaks belonging to SnO_2 and RuO_2 are missing, indicating that the reaction has reached completion. It is noteworthy that m_{SnO2} and m_{RuO2} (the slopes of the SnO_2 and RuO_2 curves, respectively) are almost identical ($m_{SnO2} = -1.3$ and $m_{RuO2} = -1.1$), and that $m_{SnO2-RuO2} = +2.5$ is close to the absolute value of the sum of m_{SnO2} and m_{RuO2}. This suggests that the reaction between SnO_2 and RuO_2 is

(27) Lodi, G.; Sivieri, E.; De Battisti, A.; Trasatti, S. *J. Appl. Electrochem.* **1978**, *8*, 135.

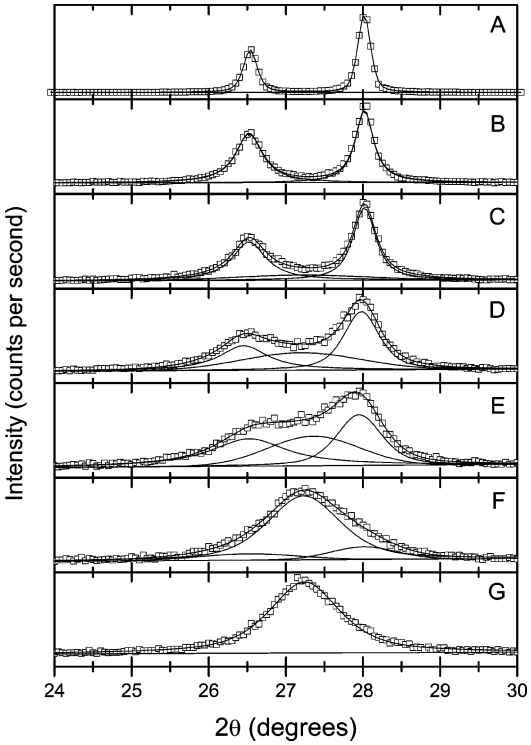

Figure 2. Expanded view of the powder XRD patterns of SnO_2−RuO_2 (50:50 wt. %) at various milling times: (A) 0 h, (B) 1 h, (C) 2.5 h, (D) 6.7 h, (E) 11 h, (F) 30.3 h, and (G) 40 h. Each pattern was fitted with three components. The open symbols are the experimental data. The contribution from each component and the fitting curve are also displayed.

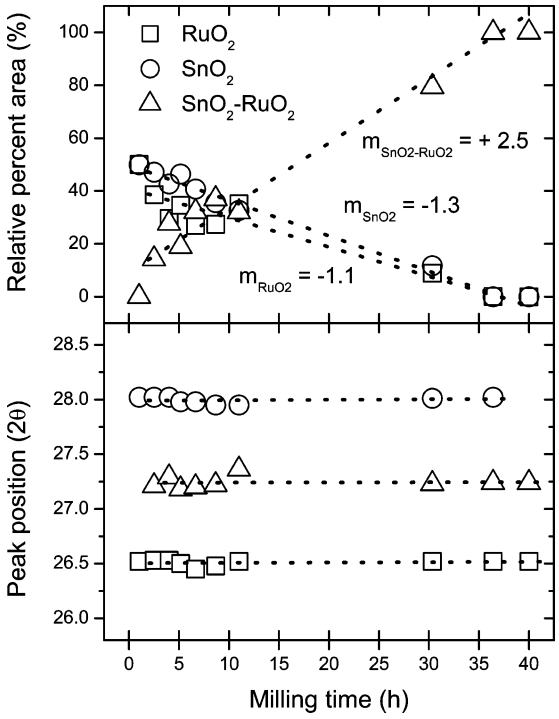

Figure 3. Peak position (lower panel) and relative percent area (upper panel) of the (110) diffraction peak of SnO_2−RuO_2 (50:50 wt. %) as a function of milling time.

stoichiometric and that SnO_2 and RuO_2 react quantitatively to form a new phase.

The peak position of each of the three components used to analyze the restricted region of the powder XRD pattern centered about the (110) peak is displayed with respect to the milling time in the lower panel of Figure 3. The peak position of each component is remarkably constant with milling time, indicating that each phase has a fixed composition that does not vary during the whole milling process. The peak located at $2\theta = 26.50$ and 27.99° corresponds to the (110) diffraction peak of SnO_2 and RuO_2, respectively. The position of the other peak (at $2\theta = 27.24°$) falls exactly between that of SnO_2 and RuO_2. This is the first indication that a solid solution of SnO_2 and RuO_2 (denoted (Sn−Ru)-O_2 hereafter) can be formed by mechanical alloying of an equimolar mixture of SnO_2 and RuO_2.

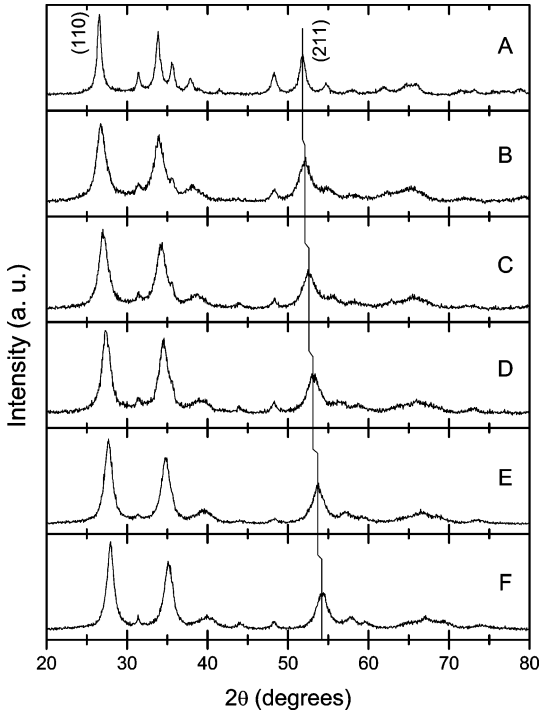

Figure 4. XRD patterns of SnO_2−RuO_2 mixtures: (A) 100:0, (B) 80:20, (C) 60:40, (D) 40:60, (E) 20:80, and (F) 0:100. The milling time was set at 40 h.

Mechanical alloying of mixtures of SnO_2 and RuO_2 were prepared, spanning the whole composition range. On the basis of the previous results, the milling time was set at 40 h. The XRD patterns of the resulting materials are shown in Figure 4. All histograms bear some close resemblance to one another. They exhibit one series of peaks that can be assigned to a tetragonal structure. The (110) peak of each sample is made of a single component, with no hint of diffraction peaks belonging to either SnO_2 or RuO_2. This indicates that the mixed oxide is a single-phased material with no trace of the starting oxides. Also, it is seen that the various (*hkl*) peaks move gradually toward the larger 2θ values as the RuO_2 content is increased from curve A to F. This effect is more clearly observed at higher 2θ values (see the curve that was drawn across the powder XRD histograms of Figure 4). This behavior suggests that the lattice parameters of the tetragonal phase decrease as the RuO_2 content is increased. After 40 h of milling, the crystallite size estimated from the width of the (110) peak is between 6 and 14 nm for all compounds.

The lattice parameters (*a* and *c*) and the volume of the unit cell of the mixed oxide were estimated from the positions

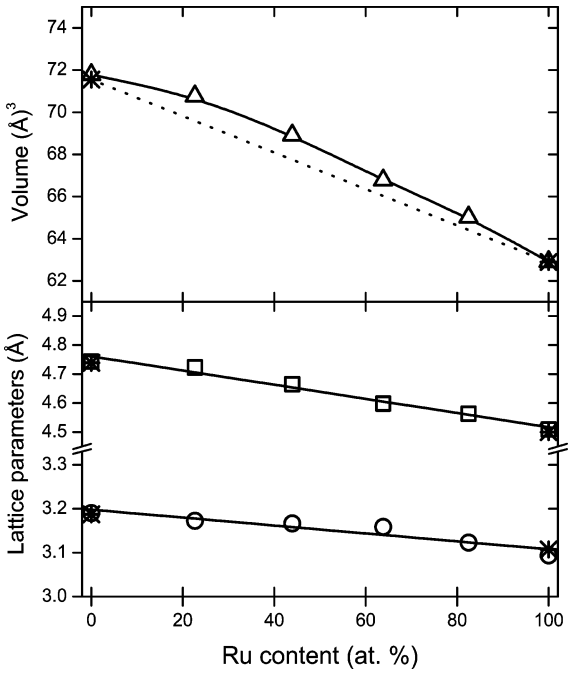

Figure 5. Evolution of the lattice parameters (*a* and *c*) and of the volume of the unit cell with the Ru content. The lattice parameters and the unit cell volume of SnO_2 (JCPDS 41-1445) and RuO_2 (JCPDS 40-1290) are also given.

of the main diffraction peaks of the tetragonal phase. As shown in Figure 5, there is a steady decrease of both *a* and *c* as the RuO_2 content of the mixed oxide increases. The ionic radius of Sn^{4+} is 0.083 nm, larger than that of Ru^{4+}, which is 0.076 nm. This difference in the ionic radius of Sn^{4+} and Ru^{4+} explains why the lattice parameters of the tetragonal cell decrease steadily as the ruthenium content increases. The volume of the tetragonal cell shows a small positive deviation from a linear behavior. These results clearly show that it is possible to form a solid solution of SnO_2 and RuO_2 over the whole compositional range with Sn^{4+} and Ru^{4+} metallic ion sharing the same cationic sublattice of the tetragonal (rutile-like) phase. From now on, these compounds will be referred to as $(Sn-Ru)O_2$, as we have established that they formed a true solid solution over the whole composition range.

There is no known phase equilibrium diagram for the SnO_2-RuO_2 system.[28] However, some conclusions about that system can be reached by looking at the known properties of very similar systems, namely RuO_2-IrO_2 and SnO_2-IrO_2. Ruthenium and iridium oxide crystallize with a tetragonal rutile-like structure with very similar lattice parameters. The unit cell dimensions of IrO_2 is $a = 4.4983$ and $c = 3.1544$ Å (JCPDS 15-870), while that of RuO_2 is $a = 4.4994$ and $c = 3.1071$ Å (JCPDS 40-1290). Also, both oxides exhibit bulk metallic conductivity. These similarities between RuO_2 and IrO_2 are reflected by the fact that both oxides readily react to form a complete solid solution over the whole compositional range.[29,30] The equilibrium phase diagram for the SnO_2-IrO_2 system in air has also been reported.[31] No intermediate binary phases exist, and only very limited solid solubility in IrO_2 was found, extending to about 3 mol % SnO_2 at 1025 °C, where dissociation occurs. Solid solution in SnO_2 was not detected. Owing to the very close similarity between the crystalline structure of IrO_2 and RuO_2, we would expect the equilibrium behavior of SnO_2-RuO_2 to be close to that of SnO_2-IrO_2, and only very limited mutual solid solubility is expected at both ends of the composition range. This is obviously not what is observed when mixed SnO_2-RuO_2 oxides are prepared by high-energy ball milling, suggesting that a metastable solid solution is formed during the alloying process.

Several attempts were made in the past to prepare mixed $(Sn-Ru)O_2$ solid solutions. However, most early attempts yielded to the formation of oxide material with more than one phase. Ito et al. reported the formation of SnO_2-RuO_2 binary oxide by a sol−gel process, although both unmixed RuO_2 and metallic Ru were found in some samples.[20] Heat-treatment of the binary oxides at elevated temperature (>600 °C) yields to phase separation, confirming the fact that SnO_2 and RuO_2 do not formed a solid solution at equilibrium. Mixed SnO_2-RuO_2 oxides have also been prepared by the thermal decomposition method, by limiting the firing temperature and the firing time.[22] However, most samples exhibit two different oxide phases, one richer in RuO_2 than the other one. In that respect, the use of high-energy ball milling to prepare mixed $(Sn-Ru)O_2$ oxide is more interesting since the resulting material is made of a single phase (the extra peaks seen in Figure 4 belong to contamination from the milling tools and are not related to the starting oxide material). Iwakura et al. also tried to prepare mixed $(Sn-Ru)O_2$ solid solution by the thermal decomposition method.[10] While the shape of the (110) diffraction peak of their compounds suggest that the material is single-phased (see Figure 6 of ref 10), the (110) peak position varies in a stepwise fashion as the RuO_2 content is varied, which is not the behavior expected if a true solid solution was formed over the whole compositional range. Instead, it was proposed that a new crystalline structure ($RuSn_2O_6$) was formed at composition (SnO_2/RuO_2) around 70:30 wt. %.[10] No evidence of this compound was found in the present study.

Morphological Characterization. Scanning electron microscopy (SEM) micrographs of $(Sn-Ru)O_2$ (20:80) are shown in Figure 6. The powder is made of large agglomerates of roughly 1-μm diameter, which are themselves composed of much smaller structures that can be as small as 50 nm (Figure 6A). This morphology is characteristic of material made by mechanical alloying. The morphology of the various samples does not vary with the RuO_2 content. In Figure 6B, the SEM micrograph of the fracture face of an electrode made from $(Sn-Ru)O_2$ (20:80) is shown. No morphological changes are induced in the powder due to the spreading process at the surface of the Ti substrate. The powder is very loosely compacted and large pores are seen throughout the thickness of the layer. The films were all about 10 μm thick.

(28) *Phase Equilibria Diagrams, 1998 Cumulative Index*. Clevinger, M. A.; Dedeno, C. L. The American Ceramic Society: Columbus, OH, 1998.
(29) McDaniel, C. L.; Schneider, S. J. *J. Res. Natl. Bur. Stand.* **1969**, *73A*, 213.
(30) Balko, E. N.; Davidson, C. R. *J. Inorg. Nucl. Chem.* **1980**, *42*, 1778.
(31) McDaniel, C. L.; Schneider, S. J. *J. Res. Natl. Bur. Stand.* **1967**, *71A*, 123.

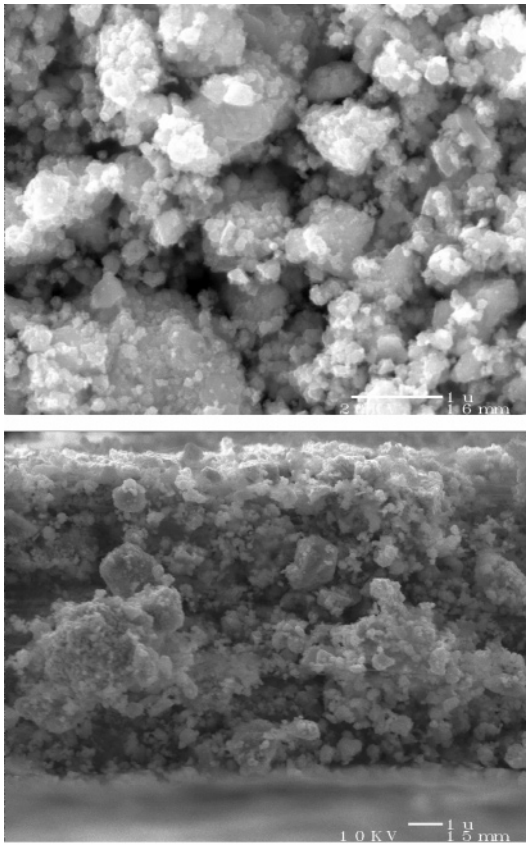

Figure 6. Scanning electron microscopy images of (Ru−Sn)O_2 (80:20): (A) powder and (B) electrode.

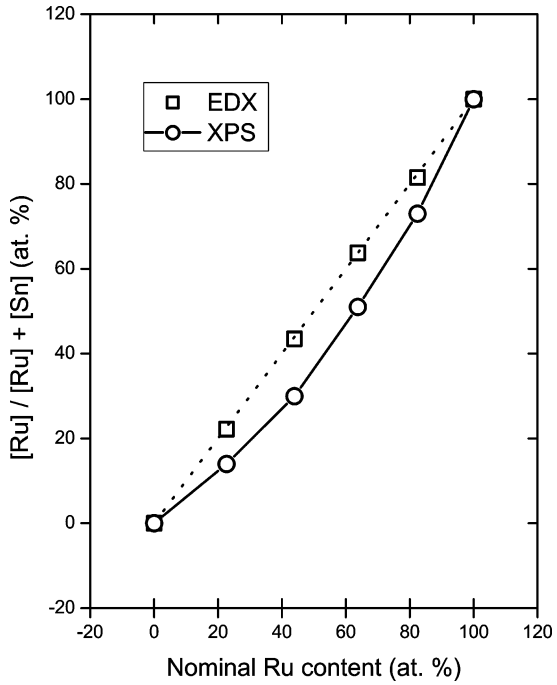

Figure 7. Bulk and surface composition of (Sn−Ru)O_2 with respect to the nominal composition of the initial mixture.

Bulk and Surface Composition. A bulk composition analysis ([Ru]/[Ru] + [Sn]) of the mixed oxide was conducted by energy dispersive X-ray analysis, and the results are given in Figure 7. There is a one-to-one correspondence between the bulk composition and the nominal Ru content, indicating there is no preferential sticking of either one of the starting oxides during the milling process.

X-ray photoelectron spectroscopy (XPS) was used to determine the surface concentration (Sn and Ru) of mixed (Sn−Ru)O_2 oxides. This determination is complicated by the fact that the binding energies of several core lines are close to each other. For example, Ru $3d_{3/2}$ (∼284 eV) and C *1s* (284.6 eV), and Ru $3p_{1/2}$ (∼484 eV) and Sn $3d_{5/2}$ (∼485 eV) core level peaks occur at almost the same binding energies. This precludes the use of these peaks for the determination of surface concentrations without going through a lengthy deconvolution procedure. Relative Sn and Ru surface concentrations were obtained by relying on the Ru $3p_{3/2}$ (∼462 eV) and Sn $3d_{3/2}$ (∼494 eV) core level peaks. That latter peak is close to that of W $4p_{1/2}$ (at ∼491 eV). However, as evidenced by the absence of any W $4p_{1/2}$ peak in pure RuO_2 milled 40 h, the amount of WC at the surface of the milled oxide is negligible. Each data set was first corrected for the nonlinear emission background by a Shirley function. Then, the total areas under the Ru $3p_{3/2}$ and Sn $3d_{3/2}$ core level peaks were used in the calculation of the surface concentrations. Since the photoelectron kinetic energies of Ru $3p_{3/2}$ and Sn $3d_{3/2}$ core level are so close, no correction was made to account for any variation in the sample thickness probed at these two energies.

The relative surface concentrations ([Ru]/[Ru] + [Sn]) as determined from XPS measurements are given in Figure 7. There is a clear Ru depletion (and a concomitant Sn enrichment) at the surface of the mixed oxide. This effect is maximum at nominal Ru content close to 50 at. %. Examples of metallic ion depletion (or enrichment) at the surface of mixed oxide materials abound in the open literature (see for example ref 3 and references therein). However, in most cases, mixed oxides are made by the thermal decomposition method. In these cases, difference in the oxidation potential of two dissimilar metallic ions could yield to an enrichment of the more easily oxidized ion during the early stage of the oxide formation, and hence a deficiency of that same species in the later stage. However, since both metallic ions are already in an oxidized form at the beginning of the preparation procedure, this mechanism cannot be responsible for the observed surface Ru depletion. Instead, difference in the ionic radii between Ru (0.076 nm) and Sn (0.083 nm) is expected to play a major role in the determination of the surface concentration. At the surface, expansion due to difference of ionic radii is more easily accommodated and segregation of Sn is observed.

Surface Electronic Structure. The Ru $3d_{5/2}$ and Ru $3d_{3/2}$ core level regions of mixed (Sn−Ru)O_2 are depicted in Figure 8. The Ru *3d* core level spectrum of (Sn−Ru)O_2 (0−100) wt. % (pure RuO_2) is characterized by a pair of relatively narrow peaks corresponding to the 5/2 and 3/2 spin−orbit components located at 280.7 eV (component 1, C1) and 284.8 eV (component 4, C4), respectively. There is also a well-defined peak at 282.5 eV (on the high binding energy side of the main Ru $3d_{5/2}$ peak) (component 2, C2), with no clearly resolvable counterpart at higher energy. The C *1s* core level peak arising from contamination of adventitious carbon is observed at 284. 8 eV (component 3, C3). This spectrum resembles closely that of crystalline RuO_2 prepared by thermal decomposition of a chloride salt solution

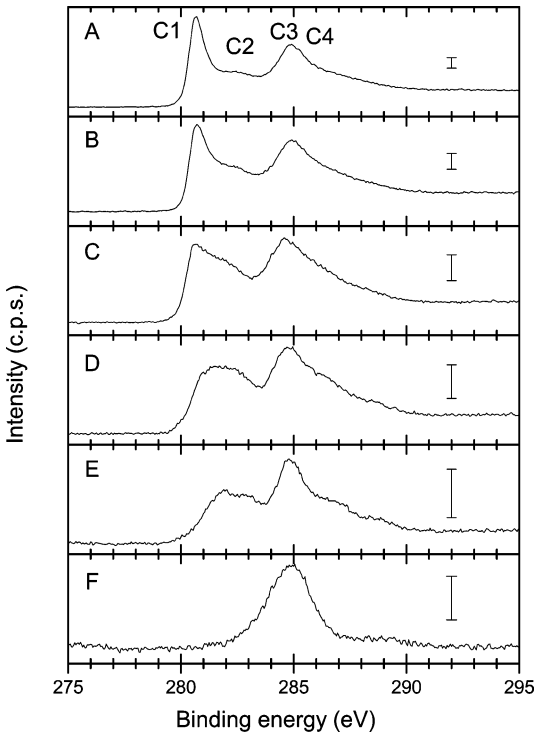

Figure 8. XPS core level spectra of mixed $(Sn-Ru)O_2$ milled during 40 h: (A) 0:100 (pure RuO_2), (B) 27:63, (C) 56:44, (D) 72:28, (E) 87:13, and (F) 100:0 at. % (pure SnO_2). The vertical bar represents 2000 counts/s in each case.

(see ref 32 and references therein). The C *1s* core level peak is the only feature seen in the core level spectrum of $(Sn-Ru)O_2$ (100−0) wt. % (pure SnO_2).

In Figure 8, the intensity ratio C1/C2 shows a marked dependency on the Ru content. While C1 is almost totally absent in $(Sn-Ru)O_2$ (87−13) at. %, the intensity of C1 is more than twice that of C2 for $(Sn-Ru)O_2$ (0−100) wt. %. For some authors,[33−36] the low and high binding energy Ru $3d_{5/2}$ core level peaks are due to the presence of two distinct oxidation states (Ru(IV) and Ru (VI), respectively), with the latter being present in the near-surface region of RuO_2. Thus, according to the mixed-valence interpretation, a decrease of the intensity ratio C1/C2 would indicate a change in the surface concentration ratio RuO_2/RuO_3. The intensity ratio C1/C2 decreases with the RuO_2 content of the sample, which would indicate that RuO_3 is preferentially formed at low RuO_2 content. This could be attributed to an oxydo-reduction reaction between RuO_2 and SnO_2 during milling, or to the fact that RuO_2 is oxidized by oxygen during the high-energy milling process. In that latter case, the presence of RuO_3 would be more easily discernible in $(Sn-Ru)O_2$ sample with low RuO_2 content due to the limited amount of oxygen molecules in the crucible. However, no evidence was found in the Sn core level peaks (not shown) suggesting reduction of tin oxide. Also, as shown in independent experiments, milling of RuO_2 in the presence of oxygen does not lead to an increase of the intensity ratio C1/C2. Finally, as we shall see later on, the cyclic voltammograms of the various $(Sn-Ru)O_2$ mixed oxides does not display any special features that would suggest that RuO_3 and reduced SnO_2 (either SnO or Sn) are present at the surface of the material.

The mixed-valence interpretation has been disputed by others.[37] According to them, the dominant, low-binding energy peak spin−orbit doublet of RuO_2 is due to screened final-state and the other doublet is due to unscreened final-state. This interpretation is consistent with the fact that (i) RuO_3 is not known to be a stable phase; (ii) nonmetallic Ru(IV) oxides have a typical Ru 3d binding energy of 282.2 eV,[37] close to the high binding energy component (C2); (iii) $Bi_{2-x}Gd_xRu_2O_7$, which changes from a semiconducting ($x = 2$) to a metallic oxide as Bi is introduced in the structure, a second spin−orbit doublet appears on the *low binding energy side* of the original doublet as the Bi content is decreased[37] (the low binding energy doublet dominates the spectra for $BiGdRu_2O_7$ and $Bi_2Ru_2O_7$); and (iv) state-specific X-ray photoelectron diffraction measurements established that photoelectrons in satellite peaks originate from atoms with the same near-neighbor structural environment as those which emit the primary photoelectrons, and that this environment is that of a rutile lattice.[38] It is highly unlikely that the near-neighbor angular distribution around Ru(VI) and Ru (IV) centers would be identical or that Ru(VI) could be accommodated in an unmodified rutile structure. Complex core level structure has also been encountered in the photoelectron spectra of several other narrow-band metallic oxides such as $LiTi_2O_4$, MoO_2, $SrMoO_3$, and NbO_2.[39] According to the final state screening interpretation, an increase of the intensity ratio C1/C2 should reflect the fact that final state screening becomes more important as the RuO_2 content is increased. This would in turn show how the electronic structure of a narrow band metallic oxide like RuO_2 is affected by partial substitution of Ru^{4+} for Sn^{4+} on the cationic sub-lattice. This interpretation will be privileged, based on the previous discussion and on the known difference between the electronic conductivity of RuO_2 and SnO_2 (the former has a metallic-like conductivity, while the latter is a large band-gap semiconductor). On the basis of this interpretation, we can conclude that the $(Sn-Ru)O_2$ solid solution extends all the way up to the very top surface of the alloy. This is in contrast to the case where the surface of the oxide could be assimilated to a composite structure made from a mixture of SnO_2 and RuO_2 (in that latter case, the Ru *3d* core level spectra of the various samples would show a close similarity to that of pure RuO_2 and only the intensity of the spectra would be expected to vary as the RuO_2 content of the milled powder is changed).

Electrochemical Properties. The voltammetric curves at 20 mV s^{-1} of $(Sn-Ru)O_2$ with various Ru contents are

(32) Rochefort, D.; Dabo, P.; Guay, D.; Sherwood, P. M. A. *Electrochim. Acta* **2003**, *48*, 4245.
(33) Kim, K. S.; Baitinger, W. E.; Amy, J. W.; Winograd, N. *J. Electron. Spectrosc. Relat. Phenom.* **1974**, *5*, 351.
(34) Kim, K. S.; Winograd, N. *J. Catal.* **1972**, *35*, 66.
(35) Lewerenz, H. J.; Stucki, S.; Kötz, R. *Surf. Sci.* **1983**, *126*, 463.
(36) Kötz, R.; Lewerenz, H. J.; Stucki, S. *J. Electrochem. Soc.* **1983**, *130*, 825.
(37) Cox, P. A.; Goodenough, J. B.; Tavener, P. J.; Telles, D.; Egdell, R. G. *J. Solid State Chem.* **1986**, *62*, 360.
(38) Kim, Y. J.; Gao, Y.; Chambers, S. A. *Appl. Surf. Sci.* **1997**, *120*, 250.
(39) Beatham, N.; Cox, P. A.; Egdell, R. G.; Orchard, A. F. *Chem. Phys. Lett.* **1980**, *69*, 479.

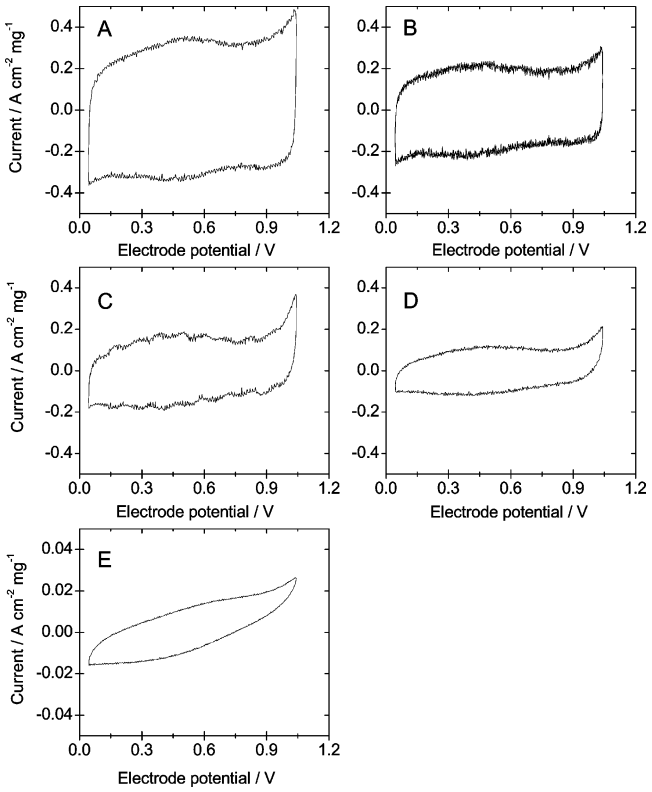

Figure 9. Voltammetric curves at 20 mV s^{-1} of (Sn−Ru)O_2 mixed oxides: (A) 0:100 at. %, (B) 27:63 at. %, (C) 56:44 at. %, (D) 72:28)at. %, and (E) 87:13 at. %. The electrolyte is 0.5 mol dm^{-3} H_2SO_4 at 25 °C.

shown in Figure 9. These voltammograms were normalized by using the amount of (Sn−Ru)O_2 oxide materials deposited on the substrate. The shape of the voltammetric curves with a Ru surface content >28 at. % is similar to that of pure (milled) RuO_2 (curve A). This behavior is expected since SnO_2 does not show any marked redox behavior in the potential range considered here. This is consistent with the fact that the open-circuit potential (E_{oc}, data not shown) of electrodes made from these materials is close to 580 mV and does not show any marked variation with the electrode composition. This indicates that the surface equilibria are dominated by Ru species. A very similar behavior was also observed in the case of IrO_2−SnO_2 mixed oxide prepared by thermal decomposition of chloride salt solution.[12]

Very large distortions of the voltammetric curves are observed if the Ru surface content is ≤13 at. % (curve E) (the CV of milled SnO_2 is not shown in Figure 9). This arises as a consequence of large uncompensated ohmic drops. Indeed, independent measurements have shown that the resistivity of the compounds increases as the Ru content decreases, with a dramatic increase for Ru content ≤13 at. %. Because the determination of the voltammetric charge is complicated by the presence of distorted voltammetric curves, the electrochemical surface properties of mixed oxides with Ru content ≤13 at. % was not considered further.

The nature of the electrochemical surface charge of (Sn−Ru)O_2 mixed oxides and its variation with the composition of the oxide was analyzed using a procedure developed by one of us.[40] It involves the determination of the voltammetric charges as a function of the sweep rates. As observed with

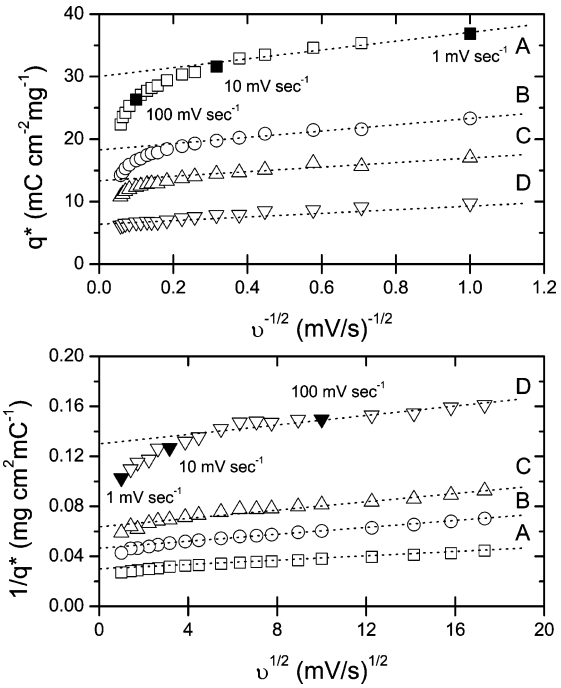

Figure 10. Dependence of the voltammetric charge of (Sn−Ru)O_2 mixed oxides on the sweep rates: (A) 0:100 at. %, (B) 27:63 at. %, (C) 56:44 at. %, and (D) (Sn−Ru)O_2 72:28 at. %. The surface concentrations determined by XPS are used to identify the various curves.

conducting oxide electrocatalysts prepared by thermal decomposition, the voltammetric charge (q^*) decreases as the potential scan rate (ν) is increased. The voltammetric charge measures the amount of protons exchanged between the oxide surface and the aqueous solution. It includes the amount of protons diffusing beneath the surface, and the occurrence of proton diffusion beneath the oxide surface can be clearly seen by means of tritium exchange experiments.[3,41] In the case of reversible redox transition, the dependence of q^* on ν is usually explained by the slow diffusion of protons into pores, cracks, and grains boundaries. Protons diffuse beneath the surface via grain boundaries, pores, cracks, and crevices, etc. Thus, proton diffusion is in fact a surface diffusion process. As the sweep rate increases, the access of protons to regions beneath the surface becomes more difficult. As ν approaches ∞, all subsurface regions are excluded and q^* tends q_O^*, which is related to the outer and more accessible active surface. Conversely, as ν approaches 0, the access to subsurface regions is fully allowed and q tends to q_T^*, which is related to the whole active surface. The difference between q_T^* and q_O^* gives q_I^*, the charge related to the inner and less accessible active sites. Therefore, for the outer surface it is meant the film regions directly facing the bulk liquid phase. For the inner surface it is meant the regions forming the walls of pores, grain boundaries, crevices, and cracks, etc.[3,40,42]

The extrapolation of q^* to $\nu = \infty$ from the q^* vs $\nu^{-1/2}$ plot (Figure 10, upper panel) gives the outer charge, q_O^*.

(40) Ardizzone, S.; Fregonara, G.; Trasatti, S. *Electrochim. Acta* **1990**, *35*, 263.
(41) Lodi, G.; Zucchini, G.; De Battisti, A.; Sivieri, E.; Trasatti, S. *Mater. Chem.* **1978**, *3*, 179.
(42) Baronetto, D.; Krstajic, N.; Trasatti, S. *Electrochim. Acta* **1994**, *39*, 2359.

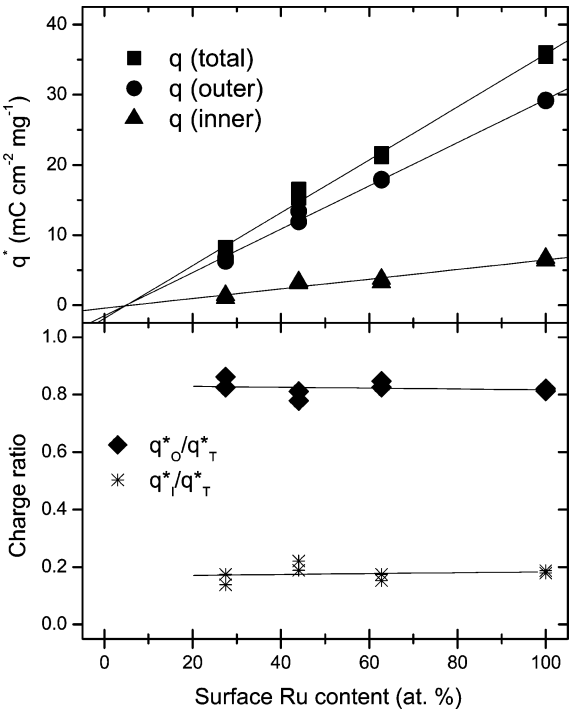

Figure 11. Evolution of total charge, outer charge, and inner charge of ($Sn-RuO_2$) mixed oxides.

The extrapolation of q^* to $\nu = 0$ from the $1/q^*$ vs $\nu^{1/2}$ (Figure 10, lower panel) gives the total charge, q_T^*. A measure of the material porosity can be obtained by computing q_I^*/q_T^*. Satisfactory linear plots are observed in Figure 10, but some deviation from a linear relationship is noted at low and high potential scan rate. At low scan rate, deviation from linearity occurs because the O_2 evolution begins at a lower electrode potential. In these conditions, also the q^* value contains a contribution from the small "tail" located on the anodic branch of the voltammetric curves. At high scan rate, distortion of the voltammetric curve occurs due to uncompensated ohmic dropt that decreases the value of q^*. Deviation from linearity is more important with increasing Ru content, possibly because the electrocatalytic activity for O_2 evolution increases with the Ru content (see below).

The effect of the surface composition of $(Sn,Ru)O_2$ on q_T^*, q_O^*, and q_I^* is depicted in Figure 11. In the case of pure RuO_2, q_T^*, q_O^*, and q_I^* are 35.3, 29.0, and 6.3 mC cm^{-2} mg^{-1}, respectively. This is consistent with data obtained elsewhere on similar materials prepared by high-energy ball milling.[43,44] In some cases, very similar values were also obtained for pure RuO_2 layer prepared by thermal decomposition,[40] although much smaller values were reached in other cases,[45] depending on the exact experimental conditions. As shown in Figure 11, q_T^*, q_O^*, and q_I^* vary linearly with the Ru surface concentrations. It must, however, be remembered that q_T^*, q_O^*, and q_I^* are determined from in situ measurements, while the Ru surface concentrations are obtained from ex situ measurements. Even if the whole approach consisting of establishing a correlation between in situ and ex situ quantities has been questioned by some authors, it must nevertheless be recognized that there is no easy way (if any) to directly assess the surface composition of an electrode by in situ measurements. Keeping that in mind, the behavior observed in Figure 11 suggests that SnO_2 acts as an inert diluent in $(Sn,Ru)O_2$, even if it is intimately mixed with RuO_2. There is no synergetic effect between Sn and Ru despite the fact that both metallic ions shared the same cationic sub-lattice of the tetragonal phase.

As shown in the lower panel of Figure 11, the ratios q^*_O/q^*_T and q^*_i/q^*_T do not vary with the surface composition of the oxide. Roughly, more than 80% of the voltammetric charge of the milled powder is associated with the outer and more easily accessible active sites, while 20% of the voltammetric charge is due to the inner and less easily accessible active site. The fact that the ratios q^*_O/q^*_T and q^*_i/q^*_T do not vary with the composition of the oxide is an indication that all materials have a similar morphology. This assertion is consistent with the fact that no difference with composition was observed in the SEM micrographs of the various oxides. It is interesting to note that for RuO_2 electrodes prepared by thermal decomposition of metal salts (e.g., $RuCl_3 \cdot 3H_2O$ on Ti platelets) only 50% of the total charge is outer charge.[40] RuO_2 electrodes prepared from thermal decomposition have a compact layer with thin deep pores meaning that active sites are more difficult to access. In the case of the nanocrystalline materials, the larger proportion of outer and more easily accessible active sites might be the result of the numerous grain boundaries present in the material which would then act as fast diffusion paths for the small H_3O^+ ions involved in the redox processes.

Finally, the electrocatalytic activity for oxygen evolution was evaluated in H_2SO_4 and anodic steady state polarization curves were recorded for all electrodes. A certain degree of irreversibility was found between the forward and backward scan, which decreases with increasing RuO_2 content. This irreversibility tended to disappear upon continuously cycling of the electrodes.

The electrocatalytic activity of the various oxide materials is best compared by following the current density at constant electrode potential. The current density, j, was evaluated at +1.15 V vs SCE. The choice of that electrode potential was dictated to mimimize the electrode potential correction due to the ohmic drop which can be quite severe as the RuO_2 content decreases. The electrocatalytic activity of an electrode depends on both electronic (structure and surface composition) and geometric (extension of the surface area) factors and knowing the real surface area is important to disentangle truly electrocatalytic (electronic) factors from mere surface area (geometric) effects. A plot of log j vs log q_T^* is shown in Figure 12. As described elsewhere by one of us,[46] if q is proportional to the Ru concentration and j is proportional to q, then we should observe a straight line of unit slope if only surface area effects are operating. This is obviously not the case for $(Sn-Ru)O_2$ materials. However, this analysis is sound provided the Tafel slope is the same for all materials.

(43) Soudan, P.; Gaudet, J.; Guay, D.; Belanger, D.; Schulz, R. *Chem. Mater.* **2002**, *14*, 1210.
(44) Rochefort, D.; Hamel, C.; Guay, D. *J. Electrochem. Soc.* **2004**, *151*, A1141.
(45) Angelinetta, C.; Trasatti, S.; Atanasoska, L. J. D.; Minevski, Z. S.; Atanasoski, R. T. *Mater. Chem. Phys.* **1989**, *22*, 231.
(46) Trasatti, S. *Electrochim. Acta* **1984**, *29*, 1503.

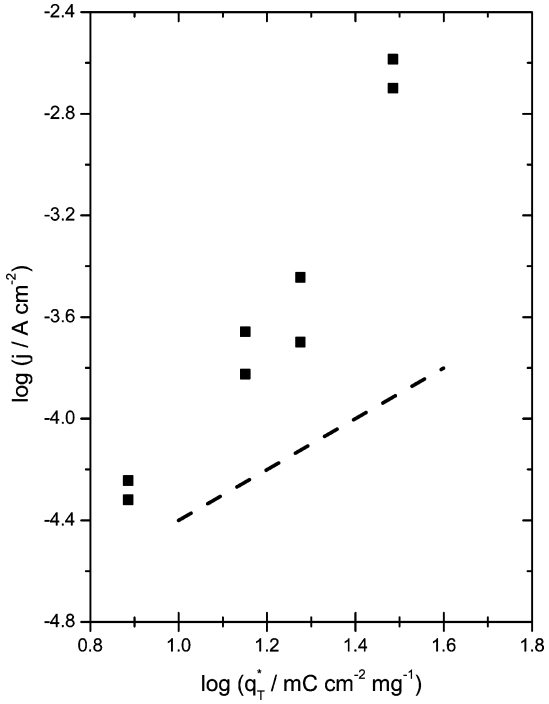

Figure 12. A log−log plot of the electrocatalytic activity (j) for O_2 evolution vs the total surface charge (q_T*) for (Sn−Ru)O_2 solid solutions.

As we shall see, this is not so in the case of these mixed oxides.

Tafel slope determined in the linear region close to the reversible oxygen potential (in the low current density region) varies with the RuO_2 content, from ∼40 mV/decade (Ru surface content = 100 and 63 at. %), to 60 mV (Ru surface content = 44 at. %), and then to 120 mV (Ru surface content = 28 at. %). The Tafel slope of 40 mV observed for Ru surface content = 100 and 63 at. % is typical of RuO_2 electrodes, and the variation observed with the composition suggests a modification of the mechanism or of its rate determining step. Since the Tafel slope depends on Ru concentration, the presence of electrocatalytic effects is already evident from such a parameter.

A complete kinetic study of oxygen evolution (including the determination of the reaction order) was not carried out, so it is not possible to establish a precise mechanism for this family of electrodes. However, an explanation for the variation of the Tafel slope with the composition can be attempted, considering the proposed generalized mechanism for oxygen evolution on oxide electrodes (see for example ref 3) and that the catalytic activity of an oxide material is related to the metal−oxygen bond strength on the surface.

According to this generalized mechanism, the first step of the oxygen evolution reaction comprises a primary discharge of water molecules (acid medium) with the oxidation of a surface active site

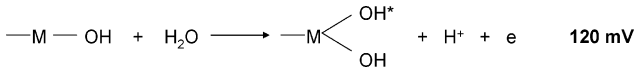

and then, the intermediate surface complex formed is converted to another more suitable intermediate

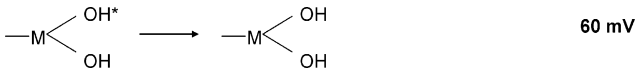

followed by its oxidation

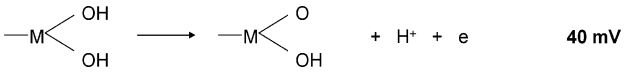

and finally O_2 is liberated from decomposition of the higher intermediate oxide.

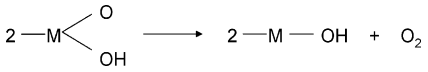

The Tafel values for each step are presented next to the respective equations, and the rate determining step for a certain oxide material is determined by the strength of interaction between the oxide surface and the oxygenated intermediates. On the basis of this mechanism it can be proposed that the variation of Tafel slope from 40 mV for RuO_2 rich samples to 120 mV for SnO_2 rich samples is due to an increased difficulty of the oxide electrode to proceed with the discharge of the first water molecule occurring with the oxidation of a surface active site. This is effectively the case for the SnO_2 phase which is an electronic insulator with no marked redox behavior in the studied potential range.

Conclusion

We have shown that metastable RuO_2−SnO_2 mixed oxides can be prepared by high-energy ball milling over the whole composition range. In these oxides, the Sn^{4+} and Ru^{4+} metallic ions share the same cationic sub-lattice of a tetragonal (rutile-like) phase, making them real (Sn−Ru)O_2 solid solutions. As revealed by X-ray photoelectron spectroscopy, this intimate mixture of Sn^{4+} and Ru^{4+} extends all the way up to the surface of the oxide. There is a slight enrichment of Sn at the surface of the oxide, which is well reflected by the electrochemically accessible surface charge showing a one-to-one correspondence with the Ru surface content of the compound.

Acknowledgment. This work was realized with the financial support of the Natural Sciences and Engineering Research Council (NSERC) of Canada. We thank the Minister of Education of Quebec for the funds received through a Quebec−Italy collaboration agreement.

CM048129L